BIOCHEMISTRY

 Volume 47, Number 4 January 29, 2008

Articles

Dynamic Structure of Disulfide-Removed Linear Analogs of Tachyplesin-I in the Lipid Bilayer from Solid-State NMR†

Tim Doherty,‡ Alan J. Waring,§ and Mei Hong*,‡

Department of Chemistry, Iowa State University, Ames, Iowa 50011, and Department of Medicine, University of California at Los Angeles, Los Angeles, California 90095

Received July 15, 2007; Revised Manuscript Received November 19, 2007

ABSTRACT: Tachyplesin-I (TP-I) is a 17-residue β-hairpin antimicrobial peptide containing two disulfide bonds. Linear analogs of TP-I where the four Cys residues were replaced by aromatic and aliphatic residues, TPX4, were found to have varying degrees of activities, with the aromatic analogs similarly potent as TP-I. Understanding the different activities of the linear analogs should give insight into the mechanism of action of TP-I. To this end, we have investigated the dynamic structures of the active TPF4 and the inactive TPA4 in bacteria-mimetic anionic POPE/POPG bilayers and compared them with the wild-type TP-I using solid-state NMR spectroscopy. ^{13}C isotropic chemical shifts and backbone (ϕ, ψ) torsion angles indicate that both TPF4 and TPA4 adopt β-strand conformations without a β-turn at key residues. ^{1}H spin diffusion from lipid chains to the peptide indicates that the inactive TPA4 binds to the membrane−water interface, similar to the active TP-I. Thus, neither the conformation nor the depth of insertion of the three peptides correlates with their antimicrobial activities. In contrast, the mobility of the three peptides correlates well with their activities: the active TP-I and TPF4 are both highly mobile in the liquid-crystalline phase of the membrane while the inactive TPA4 is completely immobilized. The different mobilities are manifested in the temperature-dependent ^{13}C and ^{15}N spectra, ^{13}C−^{1}H and ^{15}N−^{1}H dipolar couplings and ^{1}H rotating-frame spin−lattice relaxation times. The dynamics of TP-I and TPF4 are both segmental and global. Combined, these data suggest that TP-I and TPF4 disrupt the membrane by large-amplitude motion in the plane of the membrane. The loss of this motion in TPA4 due to aggregation significantly weakens its activity because a higher peptide concentration is required to disturb lipid packing. Thus molecular motion, rather than structure, appears to be the key determinant for the membrane-disruptive activities of tachyplesins.

Tachyplesin I (TP-I[1]) is a 17-residue disulfide-linked β-hairpin antimicrobial peptide found in the hemocytes of the horseshoe crab *Tachyplesus tridentatus* (*1*). It is active against a broad spectrum of Gram-negative and Gram-positive bacteria and fungi, with minimum inhibitory concentrations (MICs) from 0.3 μM to 13 μM (*2*, *3*). Compared to other β-hairpin antimicrobial peptides, TP-I is similarly effective as PG-1 and more potent than RTD-1 (*4*). The MIC

† This work is supported by the National Institutes of Health grants GM-066976 to M.H. and AI-37945 to A.J.W.

* Corresponding author. Tel: 515-294-3521, fax: 515-294-0105, e-mail: mhong@iastate.edu.

‡ Iowa State University.

§ University of California at Los Angeles.

[1] Abbreviations: TP-I, tachyplesin-I; POPE, 1-palmitoyl-2-oleoyl-*sn*-glycerol-3-phosphatidylethanolamine; POPG, 1-palmitoyl-2-oleoyl-*sn*-glycerol-3-phosphatidylglycerol.

10.1021/bi701390t CCC: $40.75
Published on Web 12/29/2007

of TP-I against the Gram-negative bacteria *E. coli* is 1 μM, and the MICs against maize fungal pathogens such as *F. graminearum* are in the range of 8−13 μM. Since peptides without disulfide bonds are easier to synthesize, linear analogs with potent activities but low toxicities are desirable. A number of structure−activity studies have been carried out on linear derivatives of TP-I, where the two disulfide bonds constraining the β-hairpin structure were removed (*3*, *5*, *6*). Interestingly, unlike the β-hairpin peptide PG-1 (*7*), several linear derivatives of TP-I retained most of the antimicrobial activities. For example, when all four cysteines were replaced by the aromatic residue phenylalanine (TPF4) or tyrosine (TPY4), the activities are comparable to those of the wild-type TP-I. The MICs of TPF4 against *E. coli* and fungal pathogens are 1 μM and 4−13 μM, respectively (*3*). This was thought to result from the retention of the β-hairpin structure in solution through aromatic ring stacking interactions, as suggested by ^{1}H NMR data (*5*). In comparison, when the cysteines were substituted by alanine (TPA4), the antimicrobial activities are significantly attenuated (*3*). The MICs against *E. coli* and fungi increased to 3 μM and >35 μM, respectively. This is thought to be related to the TPA4's random coil structure in solution (*5*). However, despite their different conformations in solution, ^{31}P NMR line shapes of glass-plate-aligned membranes show that TPY4 and TPA4 cause similar membrane disorder, which differs from the isotropic disorder caused by TP-I (*8*). When the cysteine thiol groups were protected by acetamidomethyl (Acm) groups, the linear compound TP-Acm was found to cause less dye leakage than the wild-type TP-I but more membrane perturbation, as shown by light scattering and electron microscopy data (*9*, *10*). Recently, a TP-I mutant where all cysteines were deleted and not replaced by other residues was found to retain antimicrobial activity without significant hemolytic activity (*6*). The decrease in hemolysis was attributed to a decrease of the hydrophobic character of the peptide (*11*).

While these structure−activity studies provided valuable information on the biological and physical behaviors of various tachyplesin analogs, they do not provide a cohesive understanding why some linear analogs retain significant activities while others do not. This is partly due to the fact that the three-dimensional structures of these disulfide-removed peptides in the lipid membrane are generally unknown. To identify the key molecular structural factor that determines the antimicrobial activity of tachyplesins, we undertook a solid-state NMR study of the conformation, dynamics, and depth of insertion of two tachyplesin linear analogs, TPF4 and TPA4, in lipid bilayers. TPF4 and TPA4 were chosen because of their very different activities, which should be linked to distinct structural or dynamical properties. Solid-state NMR spectroscopy is a powerful tool for obtaining atomic-level high-resolution structure information and dynamics of proteins bound to lipid bilayers (*12*, *13*). We use the anionic POPE/POPG (3:2) membrane to mimic the bacterial cell membrane. Combining conformation-dependent ^{13}C isotropic chemical shifts and backbone (ϕ, ψ) torsion angles, we find that both the active TPF4 and inactive TPA4 have a β-strand conformation without a β-turn at key positions where TP-I adopts a turn conformation. Moreover, the insertion depth of the inactive TPA4 is at the membrane−water interface, the same as the active TP-I. In comparison, the mobility of the peptides in the membrane correlate with their activities: the active TP-I and TPF4 exhibit large-amplitude motions on the NMR timescales while the inactive TPA4 is immobilized. These dynamic differences were manifested in temperature-dependent spectral intensities, motionally averaged dipolar couplings, and nuclear spin relaxation times. Thus, peptide motion in the membrane plays a central role in the antimicrobial activity of TP-I, in contrast to the well-studied β-hairpin peptide PG-1 (*13*, *14*).

MATERIALS AND METHODS

Preparation of Membrane Peptide Samples. ^{13}C- and ^{15}N-labeled amino acids were purchased from Sigma-Aldrich (Miamisburg, OH) and Cambridge Isotope Laboratory (Andover, MA) and converted to Fmoc derivatives in house. TP-I (NH_2-KWCFRVCYRGICYRRCR-$CONH_2$) was synthesized on an ABI 431A synthesizer using standard solid-phase Fmoc chemistry as described previously (*15*). After purification of the reduced peptide by HPLC, the disulfide bonds were oxidized in 0.1% acetic acid at a concentration of 0.1 mg/mL at 25 °C for 24 h. The reaction was stopped by adding acetic acid to 5% followed by purification. The linear peptides TPA4 (NH_2-KWAFRVAYRGIAYRRAR-$CONH_2$) and TPF4 (NH_2-KWFFRVFYRGIFYRRFR-$CONH_2$) were synthesized on an ABI 432A synthesizer. All peptides were purified by HPLC in an acetonitrile/water solvent system with 0.1% TFA on a Vydac C-18 reverse-phase column. MALDI mass spectrometry was used to confirm the identity of the peptides. Final purity of the peptides is greater than 95% as tested by analytical HPLC.

Three consecutive residues, G10, I11, and F12 in TPF4 and G10, I11, and A12 in TPA4, were uniformly labeled with ^{13}C and ^{15}N for measuring conformation-dependent ^{13}C isotropic chemical shifts. For TPF4, a second sample was synthesized that contained uniformly ^{13}C,^{15}N-labeled V6 and G10 and ^{15}N-labeled F7 and I11.

Isotopically labeled peptides were reconstituted into POPE/POPG (3:2) membranes by mixing the aqueous peptide solution and the lipid vesicle solution at ~298 K, above the phase transition temperature of the membrane, which is 291 K. A peptide:lipid molar ratio of 1:15 was used for all samples. The peptide−lipid mixture was ultracentrifuged at 150 000*g* to give a wet pellet, which was then lyophilized and rehydrated to 35% water by mass. This procedure produces membrane samples with low salt concentrations and well-defined hydration levels.

Solid-State NMR Experiments. All NMR experiments were carried out on a Bruker DSX-400 spectrometer (Karlsruhe, Germany) operating at a resonance frequency of 400.49 MHz for ^{1}H, 100.70 MHz for ^{13}C, and 40.58 MHz for ^{15}N. Triple-resonance MAS probes with a 4 mm spinning module was used. Low-temperature experiments were conducted using air cooled by a Kinetics Thermal Systems XR air-jet sample cooler (FTS Systems, Stone Ridge, NY). Typical cross-polarization (CP) time was 0.5 ms with a Hartman-Hahn match at 50 kHz. ^{13}C and ^{15}N 180° pulse lengths were typically 10 μs and 12 μs, respectively. ^{1}H decoupling fields of 62 kHz were used during acquisition, and 71−82 kHz were used during X-channel irradiation such as the SPC5 double-quantum period and the C−N REDOR period (see below). Recycle delays ranged from 1.5 s for frozen samples

to 2.5 s for room-temperature experiments to protect the protein from excessive radiofrequency (rf) heating. ^{13}C and ^{15}N chemical shifts were referenced externally to the α-Gly ^{13}CO signal at 176.49 ppm on the TMS scale and the *N*-acetylvaline ^{15}N signal at 122.0 ppm on the NH_3 scale.

^{13}C chemical shift of labeled sites were assigned by a combination of 2D $^{13}C-^{13}C$ correlation experiments and 1D double-quantum-filter experiments (*16*). The TPA4 experiments were carried out at 298 K while the TPF4 experiments were done at 263 K to freeze its motion. The 2D correlation experiments used the ^1H-driven ^{13}C spin diffusion pulse sequence, with a 50 ms mixing time under 8 kHz magic-angle spinning (MAS).

ψ torsion angles were measured using the NCCN technique, which correlates the $^{15}N_i-^{13}C\alpha_i$ and $^{13}CO_i-^{15}N_{i+1}$ dipolar couplings to obtain the relative orientation of the two bonds (*17*, *18*). $^{13}C\alpha-^{13}CO$ double quantum coherence was excited by the SPC5 sequence (*16*) and evolved under the $^{13}C-^{15}N$ dipolar coupling, which was recoupled by a REDOR pulse train (*19*). The SPC5 sequence used a ^{13}C rf field of 25 kHz under 5 kHz MAS. The total double-quantum excitation and reconversion time was 800 μs. For each C−N REDOR mixing time, a reference spectrum (S_0) without the ^{15}N pulses and a dephased spectrum with the ^{15}N pulses (S) were measured. S/S_0 values of the Cα or CO peak were plotted as a function of the C−N mixing time to yield the ψ-dependent curve. The NCCN experiments were conducted under 5 kHz MAS at 233 K for TPF4 and 253 K for TPA4.

The depth of insertion of TPA4 was measured using a 2D ^1H spin diffusion experiment where ^1H spin diffusion from the mobile lipid to the rigid peptide is detected via the peptide ^{13}C signals (*20*). The rate of spin diffusion depends on the $^1H-^1H$ dipolar coupling, which in turn depends on the distance between the peptide and the mobile lipid chains. The spin diffusion mixing times varied from 49 to 400 ms. A ^1H T_2 filter of 1 ms was applied before the evolution period to destroy the initial magnetization of the rigid peptide while retaining that of the mobile lipids and water. 128 t_1 points were collected in the indirect ^1H dimension. The experiments were conducted at 298 K under 4 kHz MAS. The peak heights from the 1D cross-sections at various mixing times were processed in the following way to generate the buildup curve for distance fitting: they were first corrected for ^1H T_1 relaxation during the mixing time, small drifts in the CP efficiency, and differences in the number of scans. The corrected intensities were then normalized to the water−peptide cross-peak intensity at 100 ms. The lipid−peptide cross-peak intensities were further scaled by the lipid-to-water intensity ratio in the 1D ^1H direct excitation spectrum. This accounts for the fact that even at spin diffusion equilibrium, the lipid-peptide cross-peak intensity differs from the water−peptide cross-peak intensity by a factor because of the different total magnetization of the lipid and water protons in the system.

$^{13}C-^1H$ and $^{15}N-^1H$ dipolar couplings were measured with the DIPSHIFT experiment either without (*21*) or with dipolar doubling (*22*, *23*). The doubled DIPSHIFT experiment amplifies the effect of weak couplings under MAS and was used to measure the $^{15}N-^1H$ dipolar couplings and the $^{13}C-^1H$ couplings of mobile residues with ^{13}C direct excitation. A spinning speed of 3.472 kHz was used, and an MREV-8 sequence with a ^1H 105° pulse length of 4.0 μs was used for ^1H homonuclear decoupling (*24*).

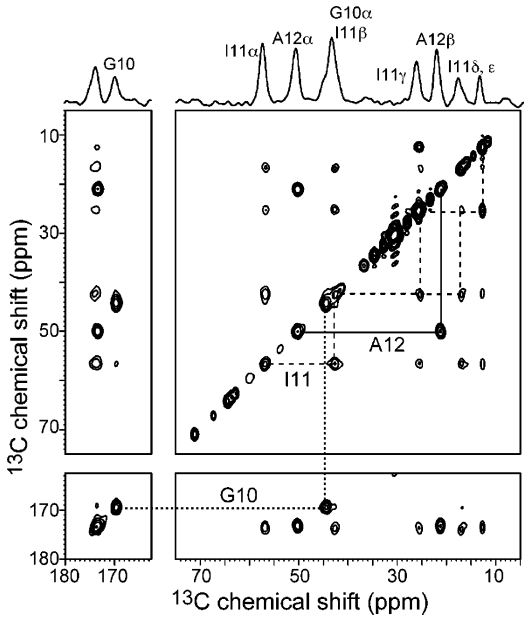

FIGURE 1: 2D $^{13}C-^{13}C$ correlation spectrum of G10, I11, A12-labeled TPA4, measured with a 50 ms mixing time under 8 kHz MAS at 298 K. Superimposed at the top is the 1D ^{13}C double-quantum filtered spectrum with the peak assignment.

The ^1H rotating-frame spin−lattice relaxation times, $T_{1\rho}$, were measured using a Lee-Goldburg spin-lock sequence with a ^1H effective spin-lock field strength of 68 kHz. A short Lee-Goldburg CP of 80 μs followed the spin lock period to achieve selective transfer of the ^1H magnetization to its directly bonded ^{13}C spin. The spin-lock experiments were conducted from 243 to 310 K at a spinning speed of 5 kHz.

RESULTS

Secondary Structure of TPA4 and TPF4. We have recently determined the conformation of TP-I in lipid bilayers through torsion angle, distance, and chemical shift constraints. These data indicate that TP-I adopts a regular β-hairpin structure in lipid bilayers, with G10 as the corner of the hairpin (*25*). In the present study, we focus on the secondary structure of the two variants, TPF4 and TPA4, to compare with the previously studied wild-type peptide. To obtain conformation-dependent ^{13}C isotropic chemical shifts we labeled residues 10−12 in TPF4 and TPA4. These residues were chosen because G10 is the center of the β-turn in the wild-type TP-I, so these residues are the most likely to adopt non-β-sheet conformations (*26*). Residue 6, Val, was also labeled in TPF4 because this site was implicated as part of a turn in TP-I and TPY4 in dodecylphosphocholine (DPC) micelles (*5*).

A representative 2D $^{13}C-^{13}C$ correlation spectrum and 1D double-quantum-filtered ^{13}C spectrum are shown in Figure 1 for TPA4 bound to POPE/POPG bilayers. The CO, Cα, and Cβ peaks are well resolved, and their isotropic chemical shifts are summarized in Supporting Information Table S1. These experimental chemical shifts are compared to the random coil shift values of Zhang et al. for each amino acid (*27*) to obtain the secondary shifts, which provide qualitative information on the backbone conformation. All labeled

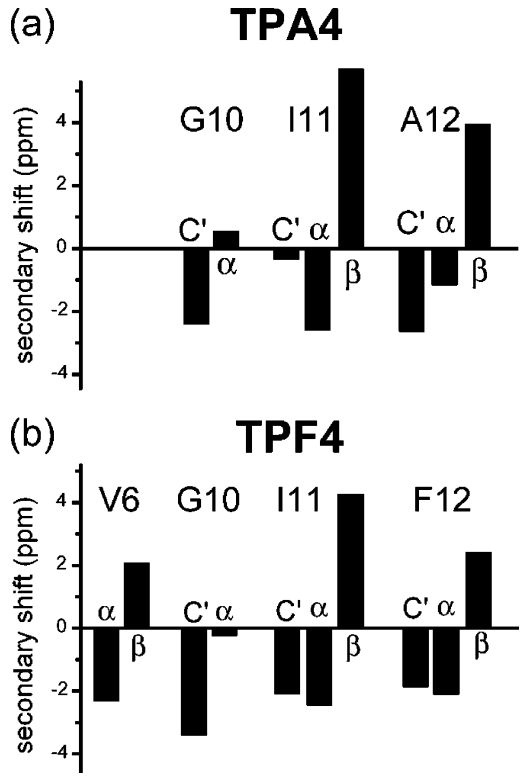

FIGURE 2: Secondary chemical shifts of CO, Cα, and Cβ for labeled residues in (a) TPA4 and (b) TPF4. Random coil shifts are taken from ref *27*.

residues in TPA4 and TPF4 give significantly negative CO and Cα secondary shifts and positive Cβ secondary shifts (Figure 2), which indicate β-strand conformation (*27*). In particular, the G10 CO chemical shifts are not close to the random coil value, suggesting that neither TPF4 nor TPA4 retain the β-turn of the wild-type peptide.

To obtain more quantitative constraints on the peptide conformation, we measured the ψ torsion angles using the NCCN technique (*17*, *18*). For a triplet of consecutively labeled residues, the ψ torsion angles of the first two residues can be measured in this way. Figure 3 shows the NCCN data. For TPA4 (a), the best-fit ψ angles are 161 ± 10° for G10 and 157 ± 5° for I11, both confirming the β-sheet conformation. If a β-turn is present, as in wild-type TP-I, then G10 would be the i+2 residue of the turn, and the maximum ψ angle possible for the i+2 residue in all types of β-turn is 80° (*28*). This is incompatible with the data, as shown by an rmsd analysis (Figure 3b). It is worth noting that the NCCN technique has the highest ψ angle resolution between 140° and 180°; thus, it detects the β-sheet conformation with high accuracy. Due to the uniaxial nature of the dipolar coupling interaction, the sign of the ψ angle can be either positive or negative. However, the negative solution can be reasonably ruled out because they fall into an unpopulated region of the Ramachandran diagram.

For TPF4 (Figure 3c,d), the G10 NCCN data is best fit by a ψ angle 160 ± 5°. Partial overlap of the I11 and F12 Cα peaks prevented the accurate extraction of the I11 ψ angle. We also measured the V6 ψ angle on a V6, F7-labeled sample and found a best-fit ψ angle of 140 ± 5° (Figure 3c). This value also falls into the β-sheet regime, consistent with the V6 secondary chemical shifts. Additional ϕ torsion angle measurements using the HNCH technique (*29*) gave a V6 ϕ angle of −140° or −100° (Supporting Information Figure S1), confirming the β-strand conformation of this residue.

Therefore, the ^{13}C chemical shifts and torsion angle results indicate that neither TPF4 nor TPA4 are bent at the G10 position where the wild-type TP-I has the β-turn. In addition, TPF4 exhibits a normal β-strand conformation at V6 in the lipid bilayer, similar to TP-I at this residue in lipid bilayers (*25*). Thus, no conformational difference exists between TPF4 and TPA4 in the lipid bilayer for the residues examined.

Membrane Binding Topology of TPA4. The membrane-bound topology of proteins, whether they are transmembrane or bound to the membrane surface, can be measured using a ^{1}H spin diffusion experiment that transfers the ^{1}H magnetization from lipids to the protein in the liquid-crystalline (LC) phase (*20*). The experiment requires that the peptide be immobilized to receive the ^{1}H magnetization from the mobile lipids and water. TPF4 is dynamic in the LC phase of the membrane (see below) and thus is not amenable to this technique, whereas TPA4 is immobilized. A representative 2D spectrum of TPA4, acquired with a spin diffusion mixing time of 400 ms, is shown in Figure 4a. The cross-peaks of interest are the lipid $(CH_2)_n$ to the peptide Cα peaks. The sum of the ^{1}H cross-sections for the peptide Cα sites are shown in Figure 4b, along with a ^{1}H direct polarization (DP) spectrum for comparison. After the cross-peak intensities are corrected for ^{1}H T_1 relaxation and normalized by the equilibrium intensity of the CH_2 peak relative to the water peak, we obtain the CH_2-to-peptide buildup curve, shown in Figure 4c. The buildup curve rises slowly and reaches about 30% of the full equilibrium intensity by 400 ms. To compare this with previously measured cases, we superimpose the best-fit buildup curves of PG-1 in the POPE/POPG membrane (dash-dotted line) and PG-1 in POPC/cholesterol membranes (dashed line) (*30*). The former represents the transmembrane case and the latter the surface-bound case, with distances of 2 Å and 25 Å, respectively, from the acyl chain ends (*30*). The TPA4 buildup curve falls between the two PG-1 limits, indicating that the peptide on average is inserted to the membrane−water interface, near the glycerol backbone and carboxyl groups of the bilayer. This approximate depth is similar to what we measured for wild-type TP-I in DMPC bilayers (*25*). Quantitative simulation of the TPA4 data gave a best-fit single distance of 5 Å from the lipid acyl chains; however, a low interfacial diffusion coefficient of 0.000125 nm^2/ms had to be used to reproduce the shape of the curve. This suggests that the insertion depth of TPA4 is somewhat heterogeneous, with a dominant fraction at a distance longer than 5 Å from the chains and a small fraction in closer contact with the chains.

Dynamics of TP Peptides in Lipid Bilayers. Since the depth of insertion of the inactive TPA4 does not differ from that of TP-I, and the conformation of the active TPF4 and inactive TPA4 are also identical, the static conformation and topology of the three TP peptides do not correlate well with their antimicrobial activities. Thus, we turn to an investigation of the dynamics of the three peptides in the lipid membrane. ^{1}H−^{13}C CP efficiency is a robust measure of the dynamic properties of molecules. Spectral intensities obtained from CP are high for immobile proteins but low for molecules undergoing large-amplitude intermediate-time scale motion.

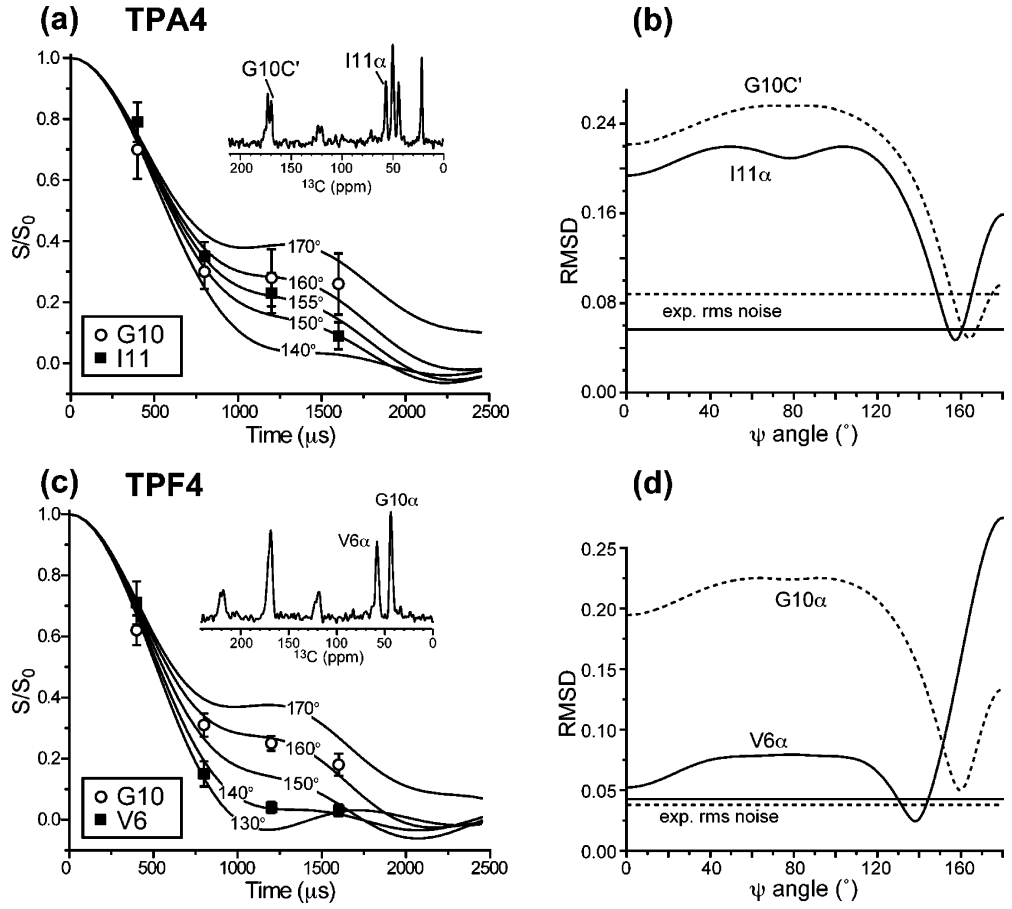

FIGURE 3: ψ torsion angles of TPA4 and TPF4 in the POPE/POPG bilayer from the NCCN experiment. (a, b) TPA4. The G10 and I11 data are best fit to ±161° and ±157°, respectively, based on the rmsd analysis in part b. (c, d) TPF4. The V6 and G10 data are best fit to ±140° and ±160°, respectively, based on the rmsd analysis in part d. Representative spectra are shown for each sample in parts a and c. The NCCN spectra were measured under 5 kHz MAS at 253 K for TPA4 and 233 K for TPF4. For comparison, the V6 ψ angle in TP-I was previously found to be ±142° (*25*).

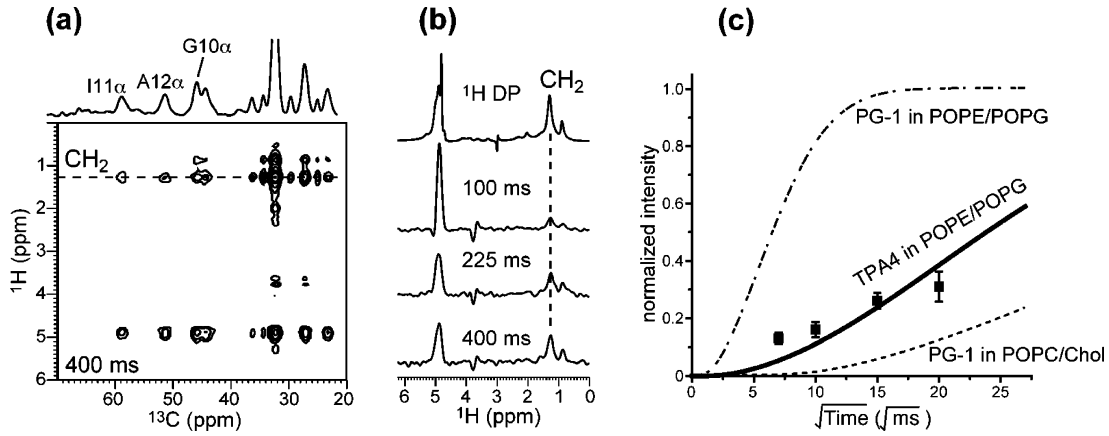

FIGURE 4: ^{13}C-detected ^{1}H spin diffusion spectra of TPA4 in the POPE/POPG membranes at 298 K. (a) A representative 2D spectrum, measured with a mixing time of 400 ms. The peptide cross-peaks to the lipid $(CH_2)_n$ are indicated by a dashed line. (b) Sum of the peptide ^{1}H cross-sections at various mixing times, compared to the directly excited ^{1}H spectrum (top). (c) The CH_2 buildup curve for TPA4 (filled symbols). Best fit (thick solid line) gives a distance of ~5 Å. The buildup curves for PG-1 in the POPE/POPG membrane (dash-dotted line) and PG-1 in the POPC/cholesterol membrane (dashed line) are shown for comparison (*30*).

If the protein reaches the fast motional limit at higher temperatures, then the CP intensities rise again. Figure 5 shows the CP spectra for the three tachyplesin peptides in the POPE/POPG membrane at 298 K (top row) and 273 K (middle row), above and below the phase transition temperature of 291 K for the POPE/POPG membrane. Both TP-I (a) and TPF4 (b) show much lower intensities at 298 K than at 273 K. This means that TP-I and TPF4 undergo anisotropic motion in the LC phase and the motion is partly frozen in the gel phase. In contrast, the TPA4 intensities (c) are little affected in this temperature range, indicating that TPA4 is already rigid in the LC phase. Even at 273 K, the TP-I and TPF4 CP intensities are still lower than TPA4, indicating that they are still more mobile than TPA4. Since all three samples were prepared with the same P/L molar ratios of 1:15, and all peptides are highly soluble in water and bind

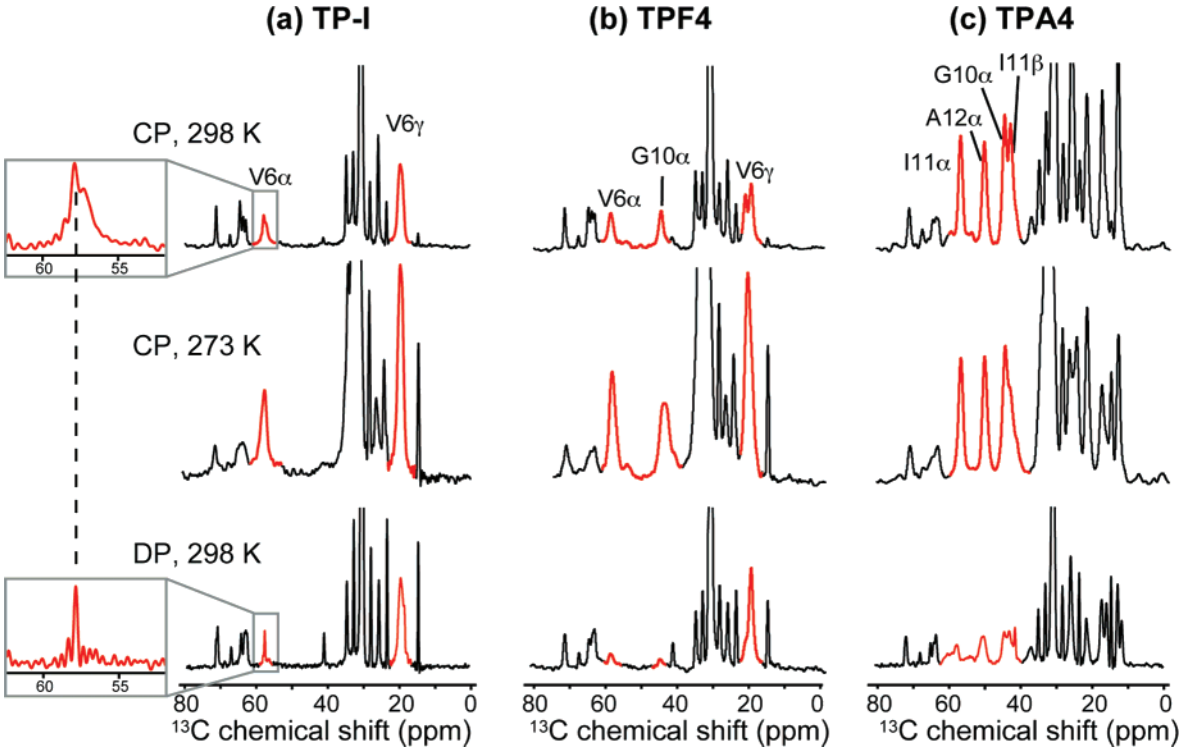

FIGURE 5: ^{13}C cross-polarization (CP) and direct polarization (DP) spectra of TP peptides in POPE/POPG membranes at 298 and 273 K. (a) TP-I, (b) TPA4, (c) TPF4. Peptide resonances are highlighted in red. The spectra are plotted to keep the lipid glycerol and headgroup signal intensities roughly constant. The TP-I and TPF4 CP intensities are weak at 298 K and much stronger at 273 K. The TPA4 CP intensity is almost not affected by the temperature. ^{13}C DP spectra (bottom) show a sharp TP-I V6α peak at 57.9 ppm. All spectra were measured under 5 kHz MAS.

to the anionic lipid bilayers with high affinity, the different dynamics result from intrinsic differences among the three peptides rather than sample preparation differences. Moreover, the immobile TPA4 is in molecular contact with the lipids, as shown by the ^{1}H spin diffusion data above; thus, it is not phase-separated from the membrane. A second TPA4 sample at a P/L ratio of 1:30 showed the same temperature-independent high CP intensities (Supporting Information Figure S2), confirming that TPA4 maintains its immobilization, which implies aggregation, even at the lower concentration.

A closer examination of the TP-I CP spectrum at 298 K shows two V6 ^{13}Cα peaks, a narrow peak at 57.9 ppm and a broad peak at 57.4 ppm. This is confirmed by the ^{13}C DP spectrum (bottom row), which shows a very narrow V6 Cα peak at 57.9 ppm. The ^{13}C T_2 of this peak is very long, about 50 ms. Thus, a small population of TP-I molecules is nearly isotropically mobile in the membrane. This V6 heterogeneous dynamics may be the result of different interactions of TP-I with the POPE and POPG lipids.

To further characterize the dynamics of the three peptides in the lipid membrane, we measured the ^{1}H rotating-frame spin−lattice relaxation times, $T_{1\rho}$, which is sensitive to molecular motions on the microsecond time scale. We measured the ^{1}H $T_{1\rho}$ using a ^{13}C-detected Lee-Goldburg spin-lock sequence with an effective spin-lock field of 68 kHz (*31*). Figure 6 compares the ^{1}H $T_{1\rho}$ relaxation decay at 298 K of the G10 ^{13}Cα site in the three peptides. TPA4 G10α shows the longest $T_{1\rho}$ of 8.4 ms while TP-I G10α has a much shorter $T_{1\rho}$ of 0.39 ms, which is more than an order of magnitude shorter than TPA4. TPF4 G10α has an intermediate $T_{1\rho}$ of 4.6 ms (Table 1). Thus, TP-I and TPF4 exhibit

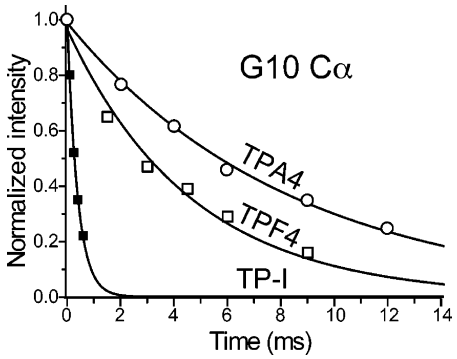

FIGURE 6: ^{13}C-detected ^{1}H rotating-frame spin−lattice relaxation of G10α in TPA4 (open circles), TPF4 (open squares), and TP-I (filled squares) at 298 K. The relaxation decay constants are 8.4, 4.6, and 0.39 ms, respectively. A ^{1}H spin-lock effective field of 68 kHz and a spinning speed of 5 kHz were used. A short ^{1}H−^{13}C LG-CP of 80 μs was used to ensure selectivity of the measured ^{1}H $T_{1\rho}$ values.

extensive motion on the 10^{-5} s time scale at 298 K while TPA4 is much less mobile.

Nuclear spin relaxation times depend both on the amplitude of motion, quantified by order parameters, and by the rates of motion on the relevant timescales. To determine whether it is primarily the amplitude or the rate that causes the different $T_{1\rho}$ relaxation times among the three tachyplesin peptides, we measured the ^{13}C−^{1}H and ^{15}N−^{1}H dipolar couplings of the labeled residues using the DIPSHIFT experiment. Reduction of the dipolar couplings from their rigid-limit values signify motion. To provide an accurate control for the order parameter calculation, we directly measured the rigid-limit couplings from crystalline model compounds under the same multiple-pulse irradiation condi-

Table 1: ^{1}H $T_{1\rho}$ Relaxation Times for the Three Tachyplesin Peptides in POPE/ POPG Membranes at 298 K[a]

peptide	site	$T_{1\rho}$, 68 kHz (ms)	$T_{1\rho}$, 40 kHz (ms)	τ_c (μs)
TP-I	V6α, 57.4 ppm	4.7 ± 0.2	2.3	3.5
	G10α	0.39 ± 0.01		
TPF4	V6α	6.6 ± 0.3	3.3	3.5
	G10α	4.6 ± 0.3	2.7	2.2
TPA4	G10α	8.4 ± 0.3	4.7	2.5
	I11α	9.1 ± 0.4	4.6	2.4
	A12α	7.6 ± 0.2	4.4	2.3

[a] Effective spin-lock fields were 68 kHz and 40 kHz. The ratio of the $T_{1\rho}$ values was used to calculate the motional correlation time τ_c as shown in ref *31*.

Table 2: ^{13}C−^{1}H and ^{15}N−^{1}H Dipolar Couplings ω_{XH}, Order Parameters S_{XH}, and rms Motional Amplitude $\langle\theta^2\rangle^{1/2}$ of Tachyplesin Peptides in POPE/POPG Membranes at 298 K

peptide	site	ω_{XH} (kHz)[a]	S_{XH}[b]	$\langle\theta^2\rangle^{1/2}$
TP-I	V6 Cα−Hα, 57.4 ppm	20.2	0.91	14°
	V6 Cα−Hα, CP, 57.9 ppm	12.8	0.57	large
	V6 Cα−Hα, DP, 57.9 ppm	3.0	0.13	large
TPF4	V6 Cα−Hα	18.1	0.81	20°
	G10 Cα−Hα	18.0	0.81	20°
	I11 Cα−Hα	17.0	0.76	23°
	I11 Cα−Hβ	11.7	0.52	large
	F12 Cα−Hα	17.0	0.76	23°
	V6 N−H	8.5	0.80	21°
	F7 N−H	9.6	0.91	14°
	G10 N−H	8.5	0.80	21°
	I11 N−H	3.2	0.30	large
TPA4	G10 Cα−Hα	22.3	1.00	0°
	I11 Cα−Hα	21.3	0.95	10°
	I11 Cα−Hβ	13.8	0.62	29°
	A12 Cα−Hα	22.3	1.00	0°
	G10 N−H	10.6	1.00	0°
	I11 N−H	9.6	0.91	14°
	A12 N−H	10.6	1.00	0°

[a] The dipolar couplings reported are the true couplings obtained by dividing the measured values by the MREV-8 scaling factor (0.47) and the doubling factor where appropriate. [b] A rigid-limit C−H coupling of 22.3 kHz and N−H coupling of 10.6 kHz were used to calculate the order parameters.

tion as the membrane peptides. The C−H dipolar couplings are resolved by the ^{13}C chemical shifts in the direct dimension of the 2D spectra. For the peptide backbone, TPA4 exhibits the strongest Cα−Hα dipolar couplings or largest C−H order parameters of 0.95−1.00 (Table 2), indicating that the motional amplitude is negligible. In contrast, the TPF4 and TP-I backbones have lower Cα−Hα order parameters of 0.57−0.91 among the detectable sites, indicating medium- to large-amplitude motions. For S_{CH} close to 1, one can calculate the root-mean-square (rms) amplitude of motion, $\sqrt{\langle\theta^2\rangle}$, according to $S_{CH} \approx 1 - (3/2)\langle\theta^2\rangle$ without assuming a specific geometry of motion. The TPA4 backbone C−H bond motional amplitude is less than 10° while TPF4 and TP-I Cα−Hα bonds have larger rms angles of greater than 14°.

To extract the N−H dipolar couplings of TPF4, we first assigned the ^{15}N peaks from ^{13}C−^{15}N 2D correlation spectra. Figure 7a shows the TPF4 ^{15}N MAS spectra from 298 to 263 K. All four labeled sites, V6, F7, G10, and I11, are resolved at 298 K, with full-widths-half-maximum of 1.4−3.3 ppm except for the low peak at 118.4 ppm, which has a line width of 4.0 ppm. As the temperature decreases, the

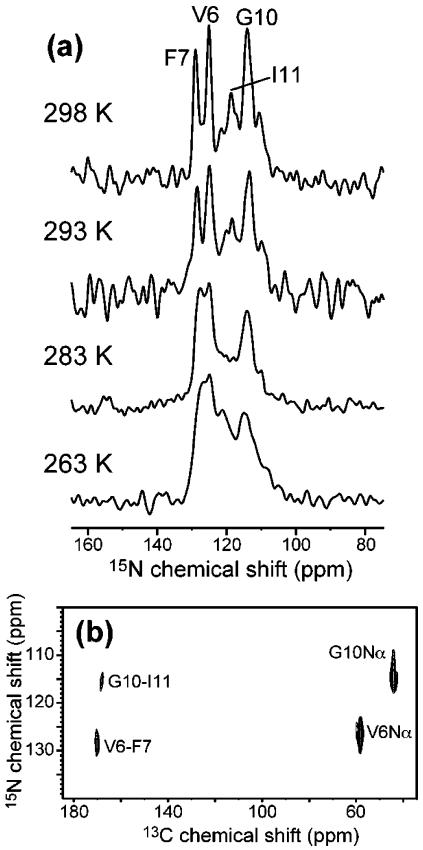

FIGURE 7: ^{15}N spectra of V6, F7, G10, I11-labeled TPF4. (a) 1D ^{15}N CP-MAS spectra as a function of temperature. Note the significant line broadening from 293 to 283 K. (b) 2D ^{15}N−^{13}C correlation spectrum at 283 K for ^{15}N resonance assignment. All spectra were measured under 5 kHz MAS. A ^{13}C−^{15}N REDOR period of 1.2 ms was used to transfer the ^{13}C and ^{15}N coherence.

^{15}N lines broaden, with a significant transition between 293 and 283 K, across the phase transition temperature of the membrane. At 283 K, the peak at 118 ppm is no longer resolved in the 1D spectrum, suggesting intermediate time scale motion at this site (*32*). A 2D ^{15}N−^{13}C correlation spectrum at 283 K allowed the assignment of all four ^{15}N peaks, with the 118 ppm peak assigned to I11 (Figure 7b).

The N−H dipolar DIPSHIFT curves of the four labeled sites in TPF4 at 298 K are shown in Figure 8. V6, F7, and G10 have N−H dipolar couplings of 8.5−9.6 kHz, corresponding to order parameters of 0.80−0.91 (Table 2), or rms angles of motion of 14−21°, while I11 has a much smaller order parameter of 0.30, indicating large-amplitude local motion.

A similar N−H order parameter measurement was carried out on TPA4, whose data are shown in Figure 9. 2D ^{13}C−^{15}N correlation spectrum allowed the assignment of all three ^{15}N−labeled sites, G10, I11, and A12. Consistent with the C−H dipolar coupling data, the N−H DIPSHIFT curves of TPA4 show near rigid-limit couplings, with order parameters of 0.91 and 1.00, which translate to small rms amplitudes of 14° and 0°, respectively.

Therefore, the dipolar order parameters of the three tachyplesin peptides decrease in the order of TPA4, TPF4, and TP-I, which is the same as the trend of decreasing ^{1}H $T_{1\rho}$ relaxation times from TPA4 to TP-I. This suggests that it is the nearly vanishing motional amplitudes, rather

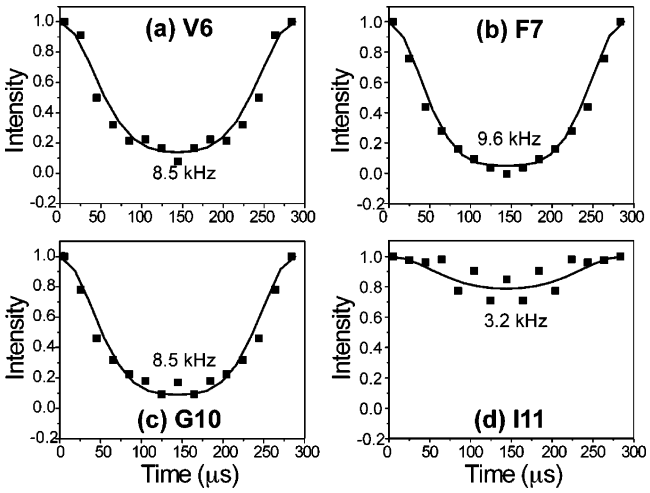

FIGURE 8: $^{15}N-^{1}H$ doubled DIPSHIFT curves of labeled sites in TPF4 at 298 K. (a) V6. (b) F7. (c) G10. (d) I11. The indicated couplings are the true values after taking into account the MREV-8 scaling factor and dipolar doubling. The data were acquired under 3.472 kHz MAS.

than slow motional rates, that give rise to the slow relaxation of TPA4. To verify this, we examined the ^{1}H $T_{1\rho}$ as a function of temperature for the three peptides (Table S2, Supporting Information). Figure 10 shows the logarithmic plot of $T_{1\rho}$ as a function of inverse temperature. TPA4 exhibits the highest $T_{1\rho}$ values, as expected. Interestingly, most sites in all three peptides are on the fast side of the $T_{1\rho}$ minimum at 298 K, indicating that their motional rates are similar and all slightly faster than the spin-lock field strength of 68 kHz. However, this fast motion has little effect on TPA4 $T_{1\rho}$ relaxation due to its miniscule amplitude. Indeed, comparing the $T_{1\rho}$ values at spin-lock field strengths of 68 kHz and 40 kHz allowed us to extract the correlation times of motion for the three peptides using a previously established procedure (*31*), and the resulting correlation times all fall into a narrow range of 2.2−3.5 μs (Table 1). This confirms that it is the amplitudes of motion, not rates, that distinguish the three tachyplesin peptides.

Figure 10 also shows that the $T_{1\rho}$ minima are broad for most sites, suggesting the presence of a distribution of motional correlation times. The only exception to the fast motional rate at 298 K and the broadness of the $T_{1\rho}$ minimum is G10α in TP-I, the only β-turn residue among all sites examined. Its $T_{1\rho}$ minimum is much lower and sharper than the other sites, and at 298 K the motional rate is slower than the spin-lock field strength of 68 kHz. We are not able to turn the corner of the minimum to the fast side without risking overheating the sample (>310 K). The particularly low $T_{1\rho}$ minimum of G10 indicates large-amplitude motion, while the shifted temperature position of the minimum indicates slower rates of motion than the other sites examined.

DISCUSSION

Among the three tachyplesin peptides studied, the antimicrobial activities are similarly strong for TP-I and TPF4 and much weaker for TPA4 (*3*). Previously, we measured the static ^{31}P spectra of oriented lipid membranes of several compositions in the presence of TP-I, TPY4, and TPA4. TP-I does not cause membrane disorder in POPC, POPC/POPG, and POPC/cholesterol membranes, but induced a significant isotropic peak in the bacteria-mimetic POPE/POPG membranes, indicating the formation of micelles or small isotropic vesicles. In contrast, the ^{31}P spectra of TPY4 and TPA4 showed an intermediate level of orientational disorder without any isotropic signals in all membranes studied. Thus, the wild-type peptide and its linear derivatives differed in the specificity of the peptide−lipid interaction and the type of membrane disorder induced, but no correlation was found between membrane orientational disorder and antimicrobial activities. In this work, we address the question of what molecular-level structural or dynamical parameters of the tachyplesin peptides account for their antimicrobial activities.

We first considered the peptide conformation in the lipid bilayer. In a previous study, we measured ^{13}C isotropic chemical shifts, torsion angles and internuclear distances to show that TP-I adopts a β-strand conformation at V6 and C7 but a β-turn conformation at G10 in lipid bilayers (*25*). This confirms solution NMR results that the two disulfide bonds constrain TP-I conformation to be a regular β-hairpin in aqueous solution and in 60 mM DPC micelles (*5*, *26*, *33*). In comparison, the present ^{13}C chemical shift and torsion angle data for TPF4 and TPA4 show that all residues examined adopt a β-strand conformation, with no sign of a β-turn at G10 (*26*, *33*). Thus, in anionic POPE/POPG bilayers, the active TPF4 and much less active TPA4 both have a β-strand conformation, which is different from the active TP-I. Thus backbone structure does not account for the activity differences among the tachyplesin peptides.

Circular dichroism data had previously shown that TPA4 is a random coil in water, 50% trifluoroethanol, and mixed phosphocholine/phosphatidic acid liposomes (*3*). Solution NMR spectra indicated that this random coil conformation of TPA4 is preserved in 320 mM DPC solution as well (*5*). These results contrast with the current β-strand conformation of TPA4 found in POPE/POPG bilayers. On the other hand, FT-IR data showed that TP-Acm adopts an antiparallel β-sheet conformation in phosphatidylglycerol lipid films (*9*). Thus, anionic lipid membranes appear to promote β-strand conformation in linear tachyplesin analogs.

We next measured the depth of insertion of TPA4 using ^{1}H spin diffusion from the lipid chains. The experiment yielded a buildup curve intermediate between full insertion into the membrane center and surface binding, indicating that TPA4 binds at the membrane−water interface. This depth of insertion is similar to that of wild-type TP-I, which we have shown by $^{13}C-^{31}P$ distances and orientation experiments to lie at the glycerol backbone and carboxyl region of the membrane, roughly parallel to the plane of the bilayer (*25*, *34*). Thus, the inactive TPA4 has the same membrane-binding topology as the active TP-I, excluding insertion depth as the cause for the different antimicrobial activities. In fact, so far partial insertion into the membrane−water interface has been found for all tachyplesin peptides, including TP-I, TP-Acm (*9*), and a cysteine-deleted mutant, CDT (*6*). Although we cannot measure the depth of insertion of TPF4 using the ^{1}H spin diffusion technique because of the dynamics of the peptide, the fact that the active TP-I shares the same topology as the inactive TPA4 is sufficient to exclude depth of insertion as the determining factor for antimicrobial activity.

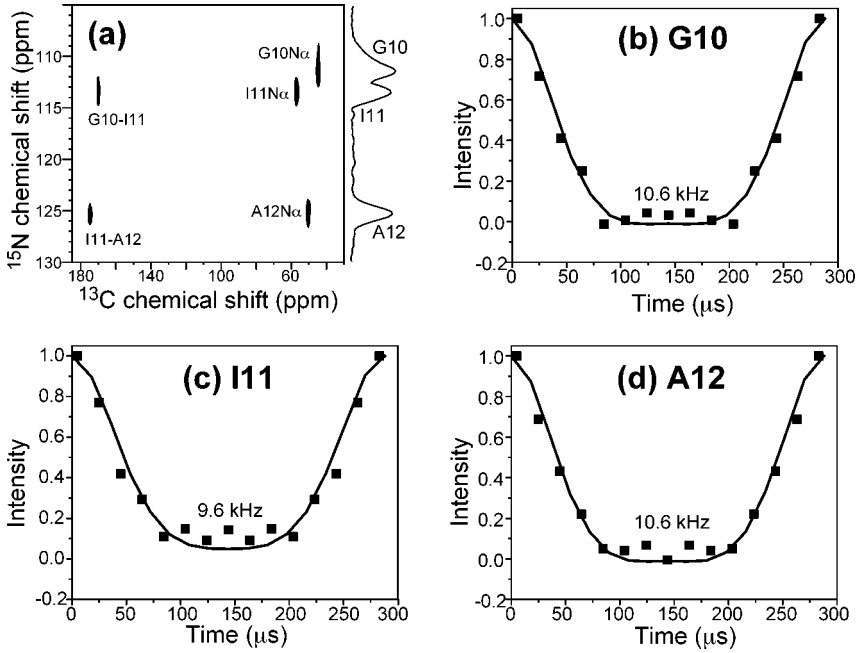

FIGURE 9: $^{15}N-^{1}H$ doubled DIPSHIFT data of TPA4 at 298 K. (a) $^{13}C-^{15}N$ 2D correlation for ^{15}N chemical shift assignment. (b−d) N−H DIPSHIFT slices of (b) G10, (c) I11, and (d) A12. The indicated couplings are the true values after dividing the fit values by the MREV-8 scaling factor and the dipolar doubling factor. The data were acquired under 3.472 kHz MAS.

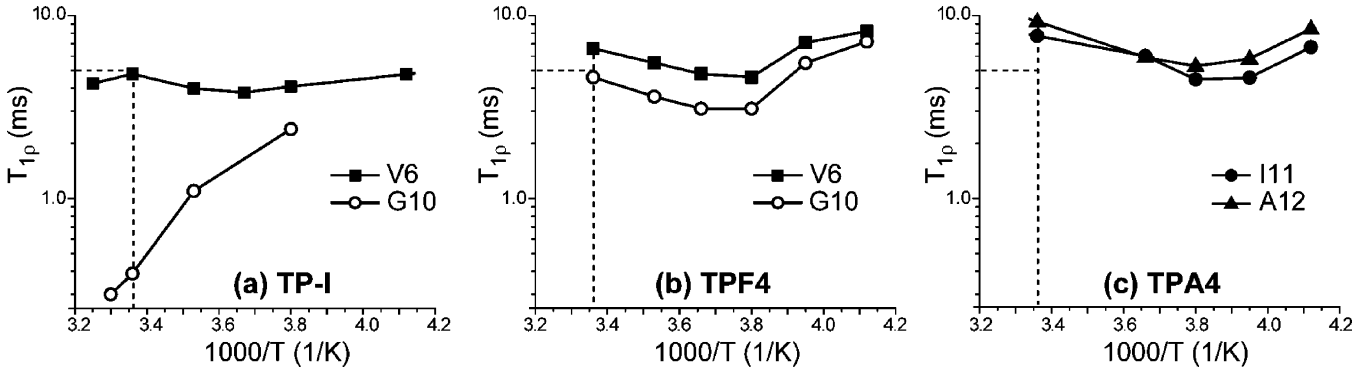

FIGURE 10: ^{13}C-detected ^{1}H $T_{1\rho}$ relaxation times of the three tachyplesin peptides as a function of temperature. (a) TP-I. (b) TPF4. (c) TPA4. The temperature of 298 K is marked by a vertical dashed line and the $T_{1\rho}$ of 5 ms is marked by a horizontal line to guide the eye for the different positions of the $T_{1\rho}$ curves among the three peptides. The V6 in TP-I corresponds to the 57.4 ppm peak in the CP spectrum, which is the most rigid component among the three V6 peaks detected (Table 2).

Finally, we turned to an examination of the dynamics of the three peptides in the POPE/POPG membrane and found a surprisingly good correlation with the antimicrobial activity: in the liquid-crystalline phase of the membrane at 298 K, TPA4 is immobile while TP-I and TPF4 undergo complex reorientational motions with significant amplitudes. This is clearly manifested in the temperature-dependent CP intensities, C−H and N−H dipolar order parameters, and ^{1}H $T_{1\rho}$ relaxation times. The loss of CP spectral intensities is a classical sign of motion on the time scale of ^{1}H decoupling fields and/or $^{1}H-^{13}C$ cross-polarization spin-lock field strengths, and has been used to assess motion in many proteins (*35*−*38*). The fact that cooling the samples to lower temperatures restored the CP intensity confirms the dynamic origin of the low intensities at higher temperature. The lack of this temperature dependence and the persistently high CP intensities of TPA4 confirm its rigid nature in the LC phase of the membrane.

The dynamics of TP-I and TPF4 show residue-specific differences and some heterogeneity among different molecules. For TP-I, three different V6 components are detected: a DP-detected peak at 57.9 ppm with a very long ^{13}C T_2 that suggests near isotropic motion, and two CP peaks at 57.9 and 57.4 ppm with C−H order parameters of 0.57 and 0.91, respectively. This heterogeneity may result from differential binding of the peptide to POPE and POPG lipids. For G10, the strikingly short ^{1}H $T_{1\rho}$ indicates large-amplitude motion of the β-turn on a time scale comparable to the spin-lock field strength of 68 kHz. In addition to these motions, we have previously observed reduced-width uniaxial static line shapes of ^{13}CO and ^{15}N-labeled sites in DLPC-bound TP-I (*34*), which indicate that TP-I undergoes global uniaxial rotation around the bilayer normal. Combining all this information, it appears that TP-I undergoes both whole-body rotational diffusion around the membrane normal and local segmental motion, with particularly large amplitude at the β-turn.

TPF4 exhibits reduced order parameters of 0.76−0.91 for most backbone sites, which translate to root-mean-square angles of ~20°. The exception is I11 N−H, which has more pronounced local motion, as manifested by its particularly low ^{15}N CP intensity and its small N−H order parameter of

0.30. The $T_{1\rho}$ data indicate that the medium- to large-amplitude motions of TPF4 have rates near the $T_{1\rho}$ minimum at 298 K, 2.2−3.5 μs. Finally, TPA4 contrasts with TP-I and TPF4 in that no measured backbone site has any significant amplitude. The motion at 298 K is thus likely very small-angle local torsional fluctuation, which is ineffective in causing relaxation.

Taken together, these NMR data indicate that the antimicrobial activities of the tachyplesin peptides are directly related to their mobilities in the lipid bilayer. While we do not know the full geometries of the motion in TP-I and TPF4, it is clear that both peptides have specific sites with large amplitudes of motion (G10 in TP-I and I11 in TPF4). In addition, global uniaxial rotation is present in TP-I. By analogy it might be present in TPF4 as well. What is also clear is that TPA4 has none of these motions. Therefore, we propose the following mechanistic model for the antimicrobial activity of the three peptides, illustrated in Figure 11. TP-I (a) and TPF4 (b) act by an "in-plane motion" model (*39*, *40*) in which the peptides, parallel to the membrane plane and immersed at the membrane−water interface, exhibit significant segmental motion as well as global motion. A few residues in these two peptides have particularly large motional amplitudes, as indicated by arrows, and may shepherd the destructive action of the peptides against the membrane. Effectively, TP-I and TPF4 behave like "stirring bars", albeit soft ones, causing transient openings in the membrane and allowing passage of water molecules and ions, thus permeabilizing the membrane. The fact that TP-I is a β-hairpin due to the disulfide bonds whereas TPF4 is mostly a β-strand does not seem to change the dynamics significantly. The presence of extensive motion suggests that both peptides form at most small oligomers. In contrast, the β-strand TPA4 is completely immobilized at the membrane−water interface. The lack of mobility is a strong indication of extensive aggregation, probably through the formation of intermolecular hydrogen bonds.

Our conclusion of TPA4 is remarkably similar to the model proposed for TP-Acm based on translocation and calcein leakage assays, FT-IR, and light scattering experiments (*9*, *10*). TP-Acm does not form pores and does not translocate across the membrane; instead, it aggregates on the membrane surface, forming interchain hydrogen-bonded β-sheets, in so doing destabilizing the bilayer organization and morphology (*10*). The ^{1}H spin diffusion data and the dynamics data shown here indicate that TPA4 aggregates and resides on the membrane surface in a similar manner to TP-Acm. The remaining antimicrobial activity of TPA4 may be mediated through the "carpet" mechanism, whose essential features are an in-plane peptide orientation at the early stage, significant aggregation, and eventual micellization of the membrane (*41*, *42*). The fact that TPA4 is much less potent than TP-I and TPF4 implies that this static aggregation-based carpet mechanism is less effective than the dynamic in-plane motion mechanism, because a higher peptide concentration is required. In other words, a mobile in-plane peptide damages the membrane more effectively than a static in-plane peptide.

The extensive dynamics of TP-I detected here are also consistent with the findings of Matsuzaki and co-workers. On the basis of electrophysiological experiments, fluorescence quenching, and calcein leakage data, they found that

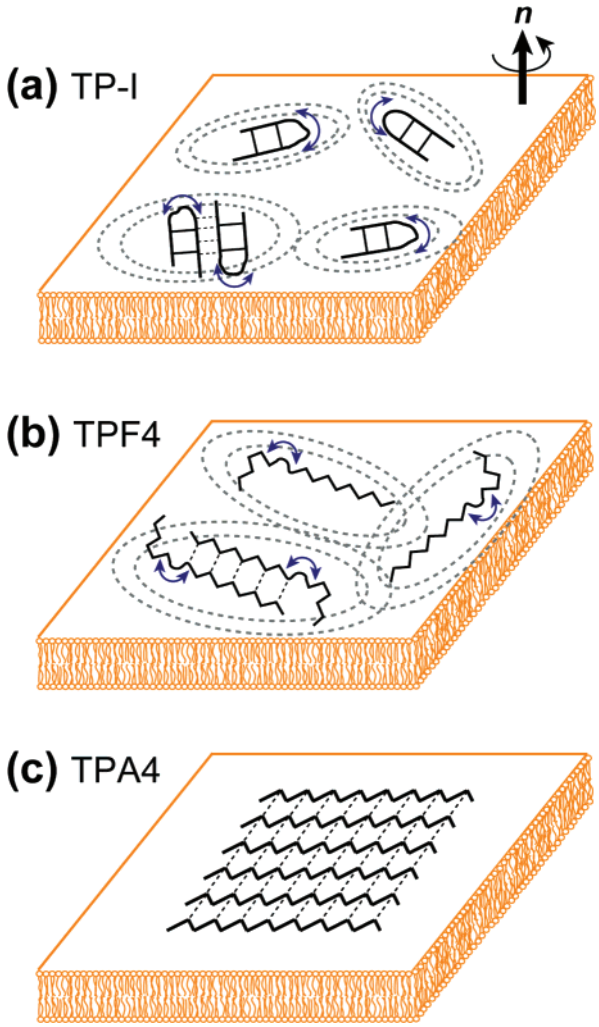

FIGURE 11: Structural models of the three tachyplesin peptides. All peptides bind to the membrane−water interface. (a) TP-I has a β-hairpin conformation and undergoes global rotational diffusion around the membrane normal and large-amplitude segmental motion at the β-turn. These extensive motions suggest that TP-I has a low oligomeric number, which is represented here schematically by a mixture of monomers and dimers. (b) TPF4. The peptide conformation is mostly although not necessarily all β-strand. The peptide exhibits dynamics similar to that of TP-I with particularly large-amplitude motion at I11. (c) TPA4 has a β-strand conformation and is completely immobilized, suggesting large-size oligomers. A higher peptide concentration is required to inflict membrane damage.

TP-I permeabilizes the lipid membrane by forming transient anion-selective pores (*9*, *10*). The peptide, initially bound to the outer membrane−water interface, translocates across the lipid bilayer. The molecular motion observed here provides a basis for the translocation and pore formation.

Interestingly, an analogous horseshoe crab antimicrobial peptide, polyphemusin, does not appear to use the same mechanism of action: it does not cause calcein leakage in POPC/POPG large unilamellar vesicles (*43*) and causes negative curvature strain (*44*). Both are opposite to the behavior of TP-I (*10*). Thus, the motional model may not apply to polyphemusin. It would be interesting to determine how small sequence changes cause differences in the behavior of these similar peptides.

The mechanism of action and structure of TP-I are also in stark contrast with those of PG-1, another cationic

β-hairpin antimicrobial peptide that we have studied extensively by NMR (*13*, *14*). PG-1 is transmembrane in most lipid membranes examined, including DLPC (*15*, *45*), POPC (*46*), and POPE/POPG (*30*) membranes. It is immobilized and oligomerized into β-barrels in POPE/POPG membranes (*30*, *47*). Thus, PG-1 exerts its membrane-disruptive action by forming long-lasting pores (*48*−*50*). In contrast, TP-I is surface-bound and does not form permanent pores (*10*) and causes membrane permeabilization by in-plane motion.

This mobility mechanism of membrane disruption may also be operative for other antimicrobial peptides. For example, the α-helical antimicrobial peptides PGLa (*51*, *52*) and ovispirin (*53*) exhibit in-plane orientation and undergo fast uniaxial rotation around the bilayer normal. This rotation is manifested by the motionally narrowed spectra of the peptides in bilayers oriented with the alignment axis perpendicular to the magnetic field.

The reason that TPF4 does not form immobile aggregates like TPA4 is unclear at this point. One possibility is that TPF4 may have non-β-sheet conformation at residues other than the ones examined here. A previous solution NMR study of TPY4 showed that in water TPY4 retains the β-hairpin fold, despite the lack of disulfide bonds, because of aromatic ring stacking interactions (*5*). Thus, it is possible that residual β-hairpin conformation may exist at other sites in TPF4 that reduces its propensity to form large aggregates. If this is true, then it would strengthen the hypothesis that it is the three-dimensional fold of the peptide in the membrane rather than the disulfide bonds themselves that is required for antimicrobial activity. Function-retaining alterations of disulfide patterns have also been observed in defensins, which are larger β-sheet analogs of TP-I (*54*).

In conclusion, we find that TP-I and TPF4 derive their antimicrobial activity from extensive motion in the plane of the lipid membrane, while TPA4 activity is significantly weakened by the fact that it is immobilized, probably due to aggregation. The β-hairpin conformation may be important for keeping the peptide from aggregating and thus maintaining the membrane-disruptive motion.

ACKNOWLEDGMENT

We thank Ms. Hattie Ziegler for help with the fitting of the TPA4 ^{1}H spin diffusion data. Tim Doherty is a recipient of a Roy J. Carver Trust predoctoral training fellowship.

SUPPORTING INFORMATION AVAILABLE

A chemical shift compilation, ^{1}H $T_{1\rho}$ relaxation times at various temperatures, V6 ϕ torsion angle data, and low-concentration TPA4 spectra are provided. This material is available free of charge via the Internet at http://pubs.acs.org.

REFERENCES

1. Nakamura, T., Furunaka, H., Miyata, T., Tokunaga, F., Muta, T., Iwanaga, S., Niwa, M., Takao, T., and Shimonishi, Y. (1988) Tachyplesin, a class of antimicrobial peptide from the hemocytes of the horseshoe crab (Tachypleus tridentatus). Isolation and chemical structure, *J. Biol. Chem. 263*, 16709−16713.
2. Tam, J. P., Lu, Y. A., and Yang, J. L. (2000) Marked increase in membranolytic selectivity of novel cyclic tachyplesins constrained with an antiparallel two-beta strand cystine knot framework, *Biochem. Biophys. Res. Commun. 267*, 783−790.
3. Rao, A. G. (1999) Conformation and antimicrobial activity of linear derivatives of tachyplesin lacking disulfide bonds, *Arch. Biochem. Biophys. 361*, 127−134.
4. Muhle, S. A., and Tam, J. P. (2001) Design of Gram-negative selective antimicrobial peptides, *Biochemistry 40*, 5777−5785.
5. Laederach, A., Andreotti, A. H., and Fulton, D. B. (2002) Solution and micelle-bound structures of tachyplesin I and its active aromatic linear derivatives, *Biochemistry 41*, 12359−12368.
6. Ramamoorthy, A., Thennarasu, S., Tan, A., Gottipati, K., Sreekumar, S., Heyl, D. L., An, F. Y., and Shelburne, C. E. (2006) Deletion of All Cysteines in Tachyplesin I Abolishes Hemolytic Activity and Retains Antimicrobial Activity and Lipopolysaccharide Selective Binding, *Biochemistry 45*, 6529−6540.
7. Harwig, S. S., Waring, A., Yang, H. J., Cho, Y., Tan, L., and Lehrer, R. I. (1996) Intramolecular disulfide bonds enhance the antimicrobial and lytic activities of protegrins at physiological sodium chloride concentrations, *Eur. J. Biochem. 240*, 352−357.
8. Doherty, T., Waring, A. J., and Hong, M. (2006) Peptide-lipid interactions of the beta-hairpin antimicrobial peptide tachyplesin and its linear derivatives from solid-state NMR, *Biochim. Biophys. Acta 1758*, 1285−1291.
9. Matsuzaki, K., Nakayama, M., Fukui, M., Otaka, A., Funakoshi, S., Fujii, N., Bessho, K., and Miyajima, K. (1993) Role of disulfide linkages in tachyplesin-lipid interactions, *Biochemistry 32*, 11704−11710.
10. Matsuzaki, K., Yoneyama, S., Fujii, N., Miyajima, K., Yamada, K., Kirino, Y., and Anzai, K. (1997) Membrane permeabilization mechanisms of a cyclic antimicrobial peptide, tachyplesin I, and its linear analog, *Biochemistry 36*, 9799−9806.
11. Dathe, M., Wieprecht, T., Nikolenko, H., Handel, L., Maloy, W. L., MacDonald, D. L., Beyermann, M., and Bienert, M. (1997) Hydrophobicity, hydrophobic moment and angle subtended by charged residues modulate antibacterial and haemolytic activity of amphipathic helical peptides, *FEBS Lett. 403*, 208−212.
12. Hong, M. (2006) Oligomeric structure, dynamics, and orientation of membrane proteins from solid-state NMR, *Structure 14*, 1731−1740.
13. Hong, M. (2007) Structure, topology, and dynamics of membrane peptides and proteins from solid-state NMR spectroscopy, *J. Phys. Chem. 111*, 10340−10351.
14. Hong, M. (2006) Solid-state NMR studies of the structure, dynamics, and assembly of beta-sheet membrane peptides and alpha-helical membrane proteins with antibiotic activities, *Acc. Chem. Res. 39*, 176−183.
15. Yamaguchi, S., Waring, A., Hong, T., Lehrer, R., and Hong, M. (2002) Solid-State NMR Investigations of Peptide−lipid Interaction and Orientation of a b-Sheet Antimicrobial Peptide, Protegrin, *Biochemistry 41*, 9852−9862.
16. Hohwy, M., Rienstra, C. M., Jaroniec, C. P., and Griffin, R. G. (1999) Fivefold symmetric homonuclear dipolar recoupling in rotating solids: application to double-quantum spectroscopy, *J. Chem. Phys. 110*, 7983−7992.
17. Costa, P. R., Gross, J. D., Hong, M., and Griffin, R. G. (1997) Solid-State NMR Measurement of psi in Peptides: a NCCN 2Q-Heteronuclear Local Field Experiment, *Chem. Phys. Lett. 280*, 95−103.
18. Feng, X., Eden, M., Brinkmann, A., Luthman, H., Eriksson, L., Graslund, A., Antzutkin, O. N., and Levitt, M. H. (1997) Direct determination of a peptide torsion angle psi by double-quantum solid-state NMR, *J. Am. Chem. Soc. 119*, 12006−12007.
19. Gullion, T., and Schaefer, J. (1989) Rotational echo double resonance NMR, *J. Magn. Reson. 81*, 196−200.
20. Huster, D., Yao, X. L., and Hong, M. (2002) Membrane Protein Topology Probed by 1H Spin Diffusion from Lipids Using Solid-State NMR Spectroscopy, *J. Am. Chem. Soc. 124*, 874−883.
21. Munowitz, M. G., Griffin, R. G., Bodenhausen, G., and Huang, T. H. (1981) Two-dimensional rotational spin-echo NMR in solids: correlation of chemical shift and dipolar interactions, *J. Am. Chem. Soc. 103*, 2529−2533.
22. Hong, M., Gross, J. D., Rienstra, C. M., Griffin, R. G., Kumashiro, K. K., and Schmidt-Rohr, K. (1997) Coupling Amplification in 2D MAS NMR and Its Application to Torsion Angle Determination in Peptides, *J. Magn. Reson. 129*, 85−92.
23. Huster, D., Yamaguchi, S., and Hong, M. (2000) Efficient b-sheet Identification in Proteins by Solid-State NMR Spectroscopy, *J. Am. Chem. Soc. 122*, 11320−11327.
24. Rhim, W.-K., Elleman, D. D., and Vaughan, R. W. (1973) Analysis of multiple-pulse NMR in solids, *J. Chem. Phys. 59*, 3740−3749.

25. Doherty, T., Waring, A. J., and Hong, M. (2006) Membrane-bound conformation and topology of the antimicrobial peptide tachyplesin I by solid-state NMR, *Biochemistry 45*, 13323−13230.
26. Kawano, K., Yoneya, T., Miyata, T., Yoshikawa, K., Tokunaga, F., Terada, Y., and Iwanaga, S. (1990) Antimicrobial peptide, tachyplesin I, isolated from hemocytes of the horseshoe crab (Tachypleus tridentatus). NMR determination of the beta-sheet structure, *J. Biol. Chem. 265*, 15365−15367.
27. Zhang, H., Neal, S., and Wishart, D. S. (2003) RefDB: A database of uniformly referenced protein chemical shifts, *J. Biomol. NMR 25*, 173−195.
28. Creighton, T. E. (1993) *Proteins: Structures and molecular properties*, 2nd ed., W. H. Freeman and Co., New York.
29. Hong, M., Gross, J. D., and Griffin, R. G. (1997) Site-resolved determination of peptide torsion angle phi from the relative orientations of backbone N−H and C−H bonds by solid-state NMR, *J. Phys. Chem. B 101*, 5869−5874.
30. Mani, R., Cady, S. D., Tang, M., Waring, A. J., Lehrer, R. I., and Hong, M. (2006) Membrane-dependent oligomeric structure and pore formation of a beta-hairpin antimicrobial peptide in lipid bilayers from solid-state NMR, *Proc. Natl. Acad. Sci. U.S.A. 103*, 16242−16247.
31. Huster, D., Xiao, L. S., and Hong, M. (2001) Solid-State NMR Investigation of the dynamics of colicin Ia channel-forming domain, *Biochemistry 40*, 7662−7674.
32. Rothwell, W. P., and Waugh, J. S. (1981) Tranverse relaxation of dipolar coupled spin systems under rf irradiation: detecting motions in solids, *J. Chem. Phys. 74*, 2721−2732.
33. Tamamura, H., Kuroda, M., Masuda, M., Otaka, A., Funakoshi, S., Nakashima, H., Yamamoto, N., Waki, M., Matsumoto, A., Lancelin, J. M., and et al. (1993) A comparative study of the solution structures of tachyplesin I and a novel anti-HIV synthetic peptide, T22 ([Tyr5,12, Lys7]-polyphemusin II), determined by nuclear magnetic resonance, *Biochim. Biophys. Acta 1163*, 209−216.
34. Hong, M., and Doherty, T. (2006) Orientation determination of membrane-disruptive proteins using powder samples and rotational diffusion: A simple solid-state NMR approach, *Chem. Phys. Lett. 432*, 296−300.
35. Rozovsky, S., and McDermott, A. E. (2007) Substrate product equilibrium on a reversible enzyme, triosephosphate isomerase, *Proc. Natl. Acad. Sci. U.S.A. 104*, 2080−2085.
36. Cady, S. D., Goodman, C., Tatko, C. D., DeGrado, W. F., and Hong, M. (2007) Determining the orientation of uniaxially rotating membrane proteins using unoriented samples: a ^{2}H, ^{13}C, and ^{15}N solid-state NMR investigation of the dynamics and orientation of a transmembrane helical bundle, *J. Am. Chem. Soc. 129*, 5719−5729.
37. Kimura, S., Naito, A., Tuzi, S., and Saito, H. (2002) Dynamics and orientation of transmembrane peptide from bacteriorhodopsin incorporated into lipid bilayer as revealed by solid state (31)P and (13)C NMR spectroscopy, *Biopolymers 63*, 122−131.
38. Perry, A., Stypa, M. P., Foster, J. A., and Kumashiro, K. K. (2002) Observation of the glycines in elastin using (13)C and (15)N solid-state NMR spectroscopy and isotopic labeling, *J. Am. Chem. Soc. 124*, 6832−6833.
39. Bechinger, B. (1997) Structure and functions of channel-forming peptides: magainins, cecropins, melittin and alamethicin, *J. Membr. Biol. 156*, 197−211.
40. Bechinger, B. (1999) The structure, dynamics, and orientation of antimicrobial peptides in membranes by multidimensional solid-state NMR spectroscopy, *Biochim. Biophys. Acta 1462*, 157−183.
41. Pouny, Y., Rapaport, D., Mor, A., Nicolas, P., and Shai, Y. (1992) Interaction of antimicrobial dermaseptin and its fluorescently labeled analogues with phospholipid membranes, *Biochemistry 31*, 12416−12423.
42. Oren, Z., and Shai, Y. (1998) Mode of action of linear amphipathic alpha-helical antimicrobial peptides, *Biopolymers 47*, 451−463.
43. Zhang, L., Rozek, A., and Hancock, R. E. (2001) Interaction of cationic antimicrobial peptides with model membranes, *J. Biol. Chem. 276*, 35714−35722.
44. Powers, J. P., Tan, A., Ramamoorthy, A., and Hancock, R. E. (2005) Solution structure and interaction of the antimicrobial polyphemusins with lipid membranes, *Biochemistry 44*, 15504−15513.
45. Buffy, J. J., Hong, T., Yamaguchi, S., Waring, A. J., Lehrer, R. I., and Hong, M. (2003) Solid-state NMR investigation of the depth of insertion of protegrin-1 in lipid bilayers using paramagnetic Mn2+, *Biophys. J. 85*, 2363−2373.
46. Buffy, J. J., Waring, A. J., Lehrer, R. I., and Hong, M. (2003) Immobilization and Aggregation of the Antimicrobial Peptide Protegrin-1 in Lipid Bilayers Investigated by Solid-State NMR, *Biochemistry 42*, 13725−13734.
47. Mani, R., Tang, M., Wu, X., Buffy, J. J., Waring, A. J., Sherman, M. A., and Hong, M. (2006) Membrane-bound dimer structure of a β-hairpin antimicrobial peptide from rotational-echo double-resonance solid-state NMR, *Biochemistry 45*, 8341−8349.
48. Mangoni, M. E., Aumelas, A., Charnet, P., Roumestand, C., Chiche, L., Despaux, E., Grassy, G., Calas, B., and Chavanieu, A. (1996) Change in membrane permeability induced by protegrin 1: implication of disulphide bridges for pore formation, *FEBS Lett. 383*, 93−98.
49. Yang, L., Weiss, T. M., Lehrer, R. I., and Huang, H. W. (2000) Crystallization of antimicrobial pores in membranes: magainin and protegrin, *Biophys. J. 79*, 2002−2009.
50. Sokolov, Y., Mirzabekov, T., Martin, D. W., Lehrer, R. I., and Kagan, B. L. (1999) Membrane channel formation by antimicrobial protegrins, *Biochim. Biophys. Acta 1420*, 23−29.
51. Glaser, R. W., Sachse, C., Durr, U. H., Wadhwani, P., Afonin, S., Strandberg, E., and Ulrich, A. S. (2005) Concentration-Dependent Realignment of the Antimicrobial Peptide PGLa in Lipid Membranes Observed by Solid-State 19F-NMR, *Biophys. J. 88*, 3392−3397.
52. Glaser, R. W., Sachse, C., Durr, U. H., Wadhwani, P., and Ulrich, A. S. (2004) Orientation of the antimicrobial peptide PGLa in lipid membranes determined from 19F-NMR dipolar couplings of 4-CF3-phenylglycine labels, *J. Magn. Reson. 168*, 153−163.
53. Yamaguchi, S., Huster, D., Waring, A., Lehrer, R. I., Tack, B. F., Kearney, W., and Hong, M. (2001) Orientation and Dynamics of an Antimicrobial Peptide in the Lipid Bilayer by Solid-State NMR, *Biophys. J. 81*, 2203−2214.
54. Dhople, V., Krukemeyer, A., and Ramamoorthy, A. (2006) The human beta-defensin-3, an antibacterial peptide with multiple biological functions, *Biochim. Biophys. Acta 1758*, 1499−1512.

BI701390T